

## **Laser Interferometer for Droplet-Sizing Application**

**D. W. Roberds, C. W. Brasier, and B. W. Bomar  
ARO, Inc.**

**July 1981**

**Final Report for Period October 1979 — September 1980**

Approved for public release; distribution unlimited.

**ARNOLD ENGINEERING DEVELOPMENT CENTER  
ARNOLD AIR FORCE STATION, TENNESSEE  
AIR FORCE SYSTEMS COMMAND  
UNITED STATES AIR FORCE**

## NOTICES

When U. S. Government drawings, specifications, or other data are used for any purpose other than a definitely related Government procurement operation, the Government thereby incurs no responsibility nor any obligation whatsoever, and the fact that the Government may have formulated, furnished, or in any way supplied the said drawings, specifications, or other data, is not to be regarded by implication or otherwise, or in any manner licensing the holder or any other person or corporation, or conveying any rights or permission to manufacture, use, or sell any patented invention that may in any way be related thereto.

Qualified users may obtain copies of this report from the Defense Technical Information Center.

References to named commercial products in this report are not to be considered in any sense as an indorsement of the product by the United States Air Force or the Government.

This report has been reviewed by the Office of Public Affairs (PA) and is releasable to the National Technical Information Service (NTIS). At NTIS, it will be available to the general public, including foreign nations.

## APPROVAL STATEMENT


This report has been reviewed and approved.



MARSHALL K. KINGERY  
Directorate of Technology  
Deputy for Operations

Approved for publication:

FOR THE COMMANDER



MARION L. LASTER  
Director of Technology  
Deputy for Operations

# UNCLASSIFIED

REPORT DOCUMENTATION PAGE		READ INSTRUCTIONS BEFORE COMPLETING FORM
1. REPORT NUMBER AEDC-TR-80-50	2. GOVT ACCESSION NO.	3. RECIPIENT'S CATALOG NUMBER
4. TITLE (and Subtitle) LASER INTERFEROMETER FOR DROPLET-SIZING APPLICATION	5. TYPE OF REPORT & PERIOD COVERED Final Report, October 1979 - September 1980	
	6. PERFORMING ORG. REPORT NUMBER	
7. AUTHOR(s) D. W. Roberds, C. W. Brasier, and B. W. Bomar, ARO, Inc., a Sverdrup Corporation Company		8. CONTRACT OR GRANT NUMBER(s)
9. PERFORMING ORGANIZATION NAME AND ADDRESS Arnold Engineering Development Center/DOT Air Force Systems Command Arnold Air Force Station, TN 37389		10. PROGRAM ELEMENT, PROJECT, TASK AREA & WORK UNIT NUMBERS Program Element 65807F
11. CONTROLLING OFFICE NAME AND ADDRESS Arnold Engineering Development Center/DOS Air Force Systems Command Arnold Air Force Station, TN 37389		12. REPORT DATE July 1981
		13. NUMBER OF PAGES 31
14. MONITORING AGENCY NAME & ADDRESS (if different from Controlling Office)		15. SECURITY CLASS. (of this report)  UNCLASSIFIED
		15a. DECLASSIFICATION/DOWNGRADING SCHEDULE N/A
16. DISTRIBUTION STATEMENT (of this Report)  Approved for public release; distribution unlimited.		
17. DISTRIBUTION STATEMENT (of the abstract entered in Block 20, if different from Report)		
18. SUPPLEMENTARY NOTES  Available in Defense Technical Information Center (DTIC).		
19. KEY WORDS (Continue on reverse side if necessary and identify by block number) interferometry laser velocimeters particle size scattering		
20. ABSTRACT (Continue on reverse side if necessary and identify by block number) A particle-sizing laser interferometer was developed for single particle, <u>in situ</u> sizing and velocity measurement of water droplets in a wind tunnel used for icing studies. Droplet diameters were in the range from 5 to 80 micrometers, flow velocity was in excess of 100 meters per second, and droplet number densities were a few hundred per cubic centimeter. Both off-axis and on-axis light collection designs were evaluated and are described. Variation of the sample volume with particle size is discussed.		

# UNCLASSIFIED

## **PREFACE**

The work reported herein was performed by the Arnold Engineering Development Center (AEDC), Air Force Systems Command (AFSC). The results of the research were obtained by ARO, Inc., AEDC Group (a Sverdrup Corporation Company), operating contractor for the AEDC, AFSC, Arnold Air Force Station, Tennessee, under ARO Project Number P32L-02B. Marshall K. Kingery, AEDC/DOT, was the Air Force project manager. The manuscript was submitted for publication on September 17, 1980.

Mr. B. W. Bomar is currently employed by Calspan Field Services, Inc., AEDC Division.

## CONTENTS

	<u>Page</u>
1.0 INTRODUCTION .....	5
2.0 THEORY OF INTERFEROMETRIC PARTICLE SIZING .....	5
3.0 OPTICS	
3.1 General .....	10
3.2 Observation Volume .....	10
4.0 ELECTRONICS	
4.1 Analog System .....	15
4.2 Digital System .....	16
5.0 DATA CORRECTIONS	
5.1 General .....	16
5.2 Sample Volume .....	18
5.3 Corrections Summary .....	21
6.0 MONOSIZE RESPONSE: THEORETICAL CONSIDERATIONS .....	22
7.0 DATA RESULTS	
7.1 Laboratory Data .....	23
7.2 Wind Tunnel Data .....	25
8.0 CONCLUSIONS .....	29
REFERENCES .....	30

## ILLUSTRATIONS

### Figure

1. Basic Schematic of Optical System .....	6
2. Theoretical and Experimental Comparison, Visibility versus $D/\delta$ for On-Axis Light Collection .....	8
3. Theoretical and Experimental Comparison, Visibility versus Diameter for Off-Axis Light Collection .....	9
4. Pedestal and a-c Magnitude versus $D/\delta$ for On-Axis Light Collection .....	12
5. Collected Light versus Particle z Coordinate, Off-Axis Light Collection .....	13
6. Pedestal versus Diameter for Off-Axis Light Collection .....	14
7. Example Log-Normal Particle Size Distribution .....	17
8. Sample Volume Cross-Sectional Area versus Particle Diameter for Off-Axis System .....	20

<u>Figure</u>	<u>Page</u>
9. Instrument Response .....	23
10. On-Axis System Response to Five Different Monosize Droplet Flows .....	24
11. Off-Axis System Response to Monosize Droplet Flow, Diameter = $9.2\ \mu\text{m}$ .....	25
12. Log-Normal Curve Fit to Measured Tunnel Size Distribution .....	26
13. Nukiyama-Tanasawa Curve Fit to Measured Tunnel Size Distribution .....	28
14. Comparison of Particle Size Interferometer with Holography Data .....	28
15. Comparison of Particle Size Interferometer with Holography Data .....	29

## 1.0 INTRODUCTION

Studies of small particles entrained in flows are of importance in a number of applications at the Arnold Engineering Development Center (AEDC). Both velocity and size distributions of particulate flows are of interest. The goal of the research reported here was the development of a particle-sizing interferometer (PSI) capable of providing both velocity and size information for use in AEDC facilities.

Specifically, a requirement existed for particle size instrumentation for the Engine Test Facility (ETF) subscale icing facility, R1D. Conditions of flow velocity (about 100 meters per second), particle number density (a few hundred per cubic centimeter), and range of particle diameters (5 to 80 micrometers) were appropriate for interferometric sizing. A PSI was developed for these conditions, and this report documents the development.

Two different systems were evaluated, one using on-axis light collection and an analog signal processor, and the other using off-axis light collection and electronics based on a commercially available high-speed transient signal digitizer. The off-axis light collection arrangement was designed to provide a smaller observation volume when it was suspected, during evaluation of the on-axis system, that signals were being received from more than one particle at a time.

The optics and electronics of the two systems are described in Sections 3.0 and 4.0 of this report, following a brief review of the theory of interferometric sizing in Section 2.0. Corrections to the raw data to eliminate system bias toward certain size ranges are the subject of Section 5.0. The system monosize response and its implications are discussed in Section 6.0. Laboratory evaluation and wind tunnel data results are presented in Section 7.0, and the performance capabilities of interferometric particle sizing are discussed with the conclusions of Section 8.0.

## 2.0 THEORY OF INTERFEROMETRIC PARTICLE SIZING

The theory of interferometric particle sizing has been developed and reported by a number of workers (Refs. 1 through 8). The optical system used is similar to a high quality, cross-beam laser velocimeter and is outlined in Fig. 1. A laser beam is split into two beams either by glass blocks or by a Bragg cell. The two beams are crossed and focused at the same location to create planar, parallel interference fringes. When a single particle crosses the interference fringes, the scattered light is collected by a lens and transmitted to a photodetector, where it is converted to an electronic signal for processing. A pinhole or slit

placed in front of the photodetector, through which the collected light is focused, eliminates stray signals originating outside the beam crossover region. The collection lens may be located either on the optical axis, as shown in Fig. 1, or at an angle off-axis. For on-axis light collection, some arrangement of beam stops or mask must be employed on the collection lens to prevent the laser source beams from entering the photodetector. A typical scattered light waveform is also shown in Fig. 1. The waveform may be thought of as having two components: a mean, or "pedestal" component (shown as a dashed line), to which is added an oscillating, or "a-c" component. The "visibility" of the fringes in the waveform is defined as the ratio of the magnitude of the a-c component at any point along the waveform to the pedestal value at that same point. The visibility may vary from point to point along the waveform.

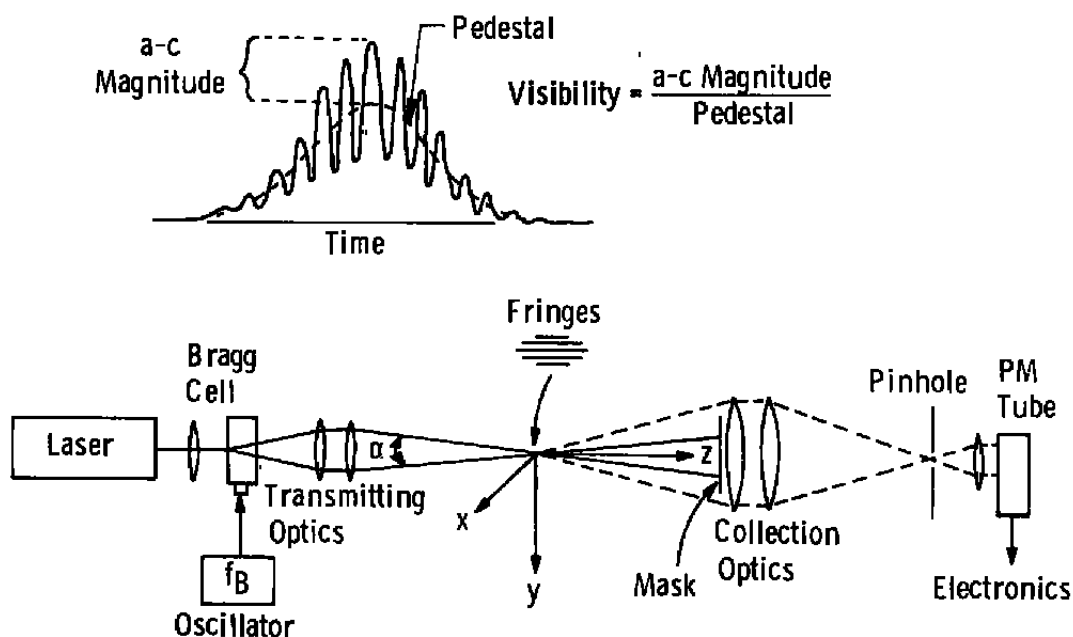


Figure 1. Basic schematic of optical system.

The scattered light signal output by the photodetector may be approximated in mathematical form as

$$i_d = i_{p0}(D) \exp \left[ -2/b_0^2 \left( x^2 + y^2 + z^2 \alpha^2/4 \right) \right] \times \left[ \cosh \left( 2yz \alpha / b_0^2 \right) + V_0 \cos \left( 2\pi y / \delta + 2\pi f_B t \right) \right] \quad (1)$$

where  $x, y$ , and  $z$  are coordinates of the particle location with respect to the axes shown in Fig. 1,  $b_0$  is the laser beam waist radius in the crossover region,  $\alpha$  is the full beam separation



angle (assumed small),  $f_B$  is the Bragg cell driving frequency (set equal to zero if a glass block beam splitter rather than a Bragg cell is used),  $\delta$  is the fringe spacing,  $V_o$  is the maximum, or peak value reached by the visibility along the waveform, and  $t$  is time. The variable  $i_{po}(D)$  is the value of the pedestal when the particle is centered at  $x = y = z = 0$ . It is a function of the particle diameter,  $D$ , laser power, light collection optics geometry, and photodetector and electronic gain; but for the interest here, only its dependence on particle diameter,  $D$ , is indicated.

The ratio of the a-c (i.e., the cosine) magnitude to the pedestal gives the visibility,  $V$ , as follows:

$$V = V_o / \cosh \left( 2y z a / b_o^2 \right) \quad (2)$$

A previously published technical report (Ref. 9) has shown how the peak visibility,  $V_o$ , may be related to the particle size for a given collection optics geometry. The theory was developed using Fraunhofer diffraction and therefore applies to light collected on-axis in the forward direction. The size of the collection aperture and beam stop was taken into account. Other authors (Refs. 4 through 7) have used the Mie theory of scattering from spheres to predict visibility versus particle diameter for off-axis light collection and for particles too small for scalar diffraction theory to apply. A recently published paper (Ref. 10) reports the use of ray optics to relate off-axis visibility to droplet diameter for large refracting droplets.

Curves relating peak visibility to the ratio of particle diameter to fringe spacing ( $D/\delta$ ) are shown in Fig. 2 for two different, on-axis receiving apertures. The dashed curve to the left is for the theoretical case where all of the forward-scattered light is collected (corresponding to an infinite collection lens diameter and no beam stops). The solid curve to the right is for the aperture created by placing on the collection lens a specialized mask which admits light only through two 60-deg, wedge-shaped openings at the top and bottom of the lens as sketched in the upper right of the figure. This curve was calculated using scalar diffraction theory [Eq. (13), Ref. 9] and assumes spherical scatterers with diameters much larger than the illuminating wavelength. Each of the two curves shown is useful for sizing over roughly a 10:1 size range. At the upper end of the size range, ambiguity results from the fact that more than one particle size has the same visibility. At the lower end of the size range, the curve becomes too flat and insensitive to size changes to be usable.

The fringe spacing is chosen for the particular particle size range of interest and the applicable visibility curve. For example, when a 60-deg mask is used, the value  $D/\delta = 2$  lies at the upper end of the usable size range, whereas for the dashed curve of Fig. 2, the value  $D/\delta = 1$  lies near the upper end of the size range. Therefore, to cover a given size range, the

60-deg mask uses a fringe spacing about half that of a system having a visibility curve similar to the dashed one.

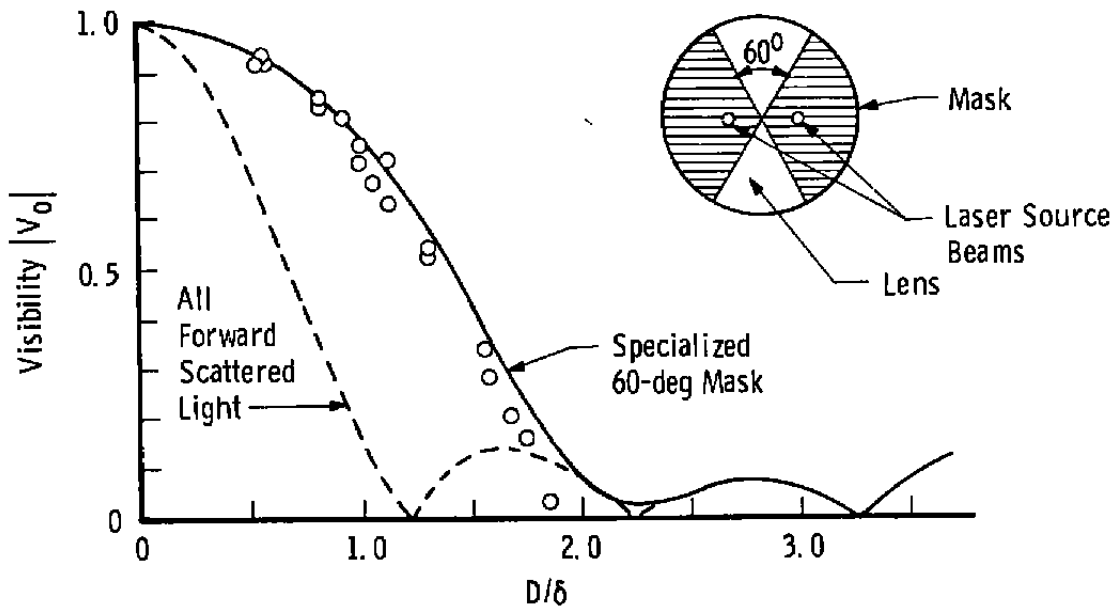


Figure 2. Theoretical and experimental comparison, visibility versus  $D/\delta$  for on-axis light collection.

Experimental data obtained using glass spheres placed on a glass slide are shown for comparison with the 60-deg mask curve. Each glass sphere was sized using the distance from the center to one of the concentric rings in its single beam diffraction pattern for comparison with the corresponding visibility measurement.

For light scattered near the optical axis in the forward direction from large particles such as those in the size range of interest here, there is minimal dependence on the scattering particle's index of refraction. Experimental data agree well with the results of scalar diffraction theory, arrived at independently of the refractive index.

A curve relating visibility to droplet diameter for a case where the scattered light is collected off-axis is shown in Fig. 3. The collection aperture used is shown in the upper right of the figure. The collection lens is centered 12 deg off-axis in a direction perpendicular to the plane of the beams; the lens diameter subtends an angle of 11.4 deg at the center of the beam crossover region. The curve was calculated using Mie theory for the case of water droplets (refractive index = 1.33), an illuminating wavelength of  $\lambda = 0.5145 \mu\text{m}$ , and a beam separation angle of  $\alpha = 2.7$  deg, which gives a fringe spacing of  $\delta = 11 \mu\text{m}$ . The

illuminating beams were assumed to be linearly polarized in the x direction (i.e., perpendicular to the plane of the beams). A curve calculated for the case of oleic acid droplets (refractive index = 1.46) closely follows the curve for water in the range of diameters from 5 to 30  $\mu\text{m}$ .

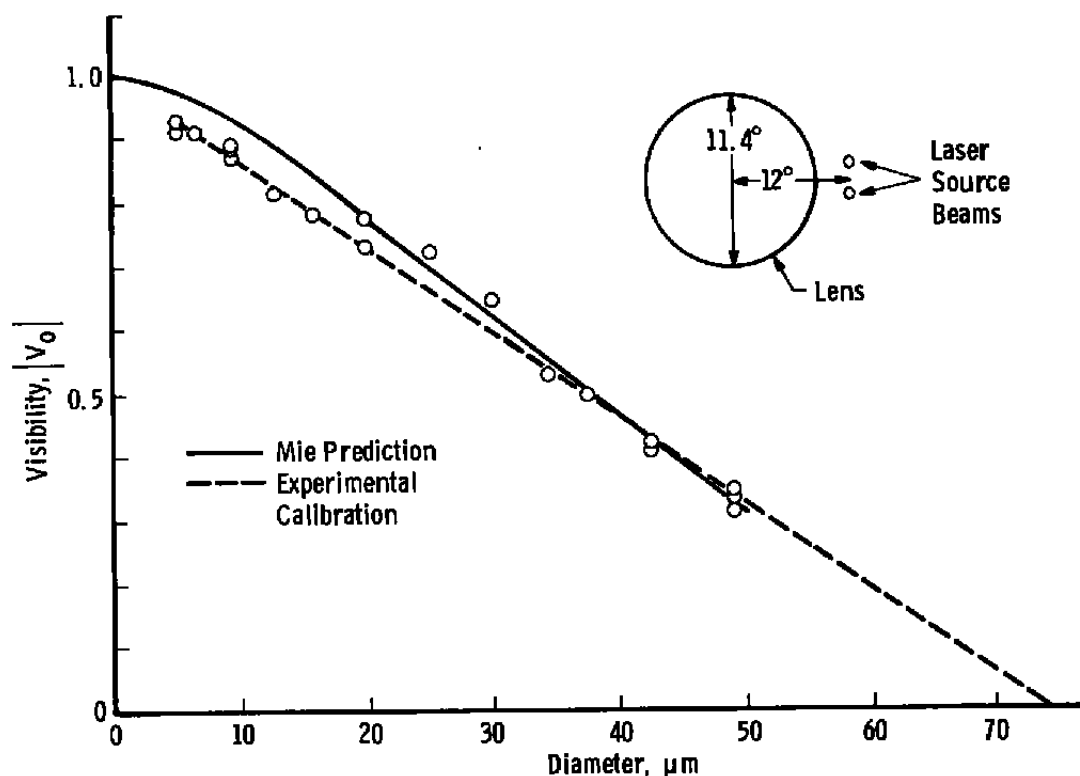


Figure 3. Theoretical and experimental comparison, visibility versus diameter for off-axis light collection.

The experimental data shown were obtained using water droplets and oleic acid droplets produced by a Berglund-Liu vibrating orifice particle generator. The diameter of the droplets in the monosize (monodisperse) stream produced by the generator could be calculated accurately from the liquid flow rate and the vibration frequency of the orifice (Ref. 11). The data points shown are centers of distribution (histogram modes) measured in response to monosize droplets flowing through the beam crossover region.

The experimental data fall noticeably below the theoretical curve for the smaller droplet diameters. This is probably due to imperfect fringe contrast in the beam crossover region. The calibration curve which was used in wind tunnel tests to relate visibility to particle size for the off-axis system is shown as the dashed straight line and is based on the experimental data.

### 3.0 OPTICS

#### 3.1 GENERAL

Both an optical system using on-axis light collection and an optical system using off-axis light collection were built and evaluated. Both systems consisted of two major units, one a transmitting optics package for generating a set of high-contrast fringes, and the other a collection optics package for collecting the scattered light. In both systems the laser beams were crossed and focused at a point 100 cm in front of the final transmitting lens to form the interference fringe set. The collection lenses were a set of 15-cm-diam, f5 lenses, giving a total system "throw" of 1.75 m between the transmitting and receiving units.

The on-axis system used a 15 mw, helium-neon laser operating in the TEM<sub>00</sub> mode at a wavelength of 0.6328  $\mu\text{m}$ , a Bragg cell driven at 15 MHz to split the beams, and a system of lenses to cross and focus the beams at a common point to produce a set of moving fringes. In the wind tunnel application the fringes moved in a direction opposite to the direction of particle flow to accommodate the electronics. In the laboratory, a stationary particle could be positioned at the crosspoint with the fringes moving past the particle to produce signals for calibration purposes. The primary fringe spacing was designed for 26  $\mu\text{m}$  with the capability of obtaining other selected fringe spacings by changing lenses. The beam waist diameter was 150  $\mu\text{m}$ .

Collection optics for the on-axis system included the specialized mask with 60-deg wedge-shaped openings, a 200- $\mu\text{m}$ -diam pinhole to block light originating at points other than the beam crossover region, and an RCA 8644 photomultiplier tube.

The off-axis system used a 150-mw Argon ion laser operating at a wavelength of 0.5145  $\mu\text{m}$ . The beams were split using path-length-compensated glass blocks, which produced stationary fringes in the beam crossover region. The fringe spacing used was 11  $\mu\text{m}$ , and the beam waist diameter was 200  $\mu\text{m}$ .

Scattered light for the off-axis system was collected in accordance with the arrangement of Fig. 3. The light was focused through a slit 120  $\mu\text{m}$  wide before being detected by an RCA C30872 avalanche photodiode.

#### 3.2 OBSERVATION VOLUME

Interferometric sizing requires that there be only one particle at a time in the field of view of the optical system. Extraneous signals from large particles crossing the beams, even

outside the beam crossover region, can interfere with the measurement of a small particle located within the crossover region. This leads to the concept of a loosely defined "observation volume" which must be empty of additional particles when a particle is in the crossover region and a measurement is being made. For a first-order approximation of the requirements which must be imposed on the size of the observation volume for a given density,  $n$ , of particles in the flow, the assumption is made that the observation volume,  $V_{ob}$ , is cylindrical, of radius  $b_o$  equal to the beam radius in the crossover region, and of length  $z_{ob}$ , so that  $V_{ob} = \pi b_o^2 z_{ob}$ . It is further assumed that the probability of occurrence of multiple particles is sufficiently small if the expected number of particles at any time in the observation volume, given by  $nV_{ob}$ , is 0.1 or less. (Using a Poisson distribution of events to calculate the probability of finding two or more particles in the observation volume, given that there is already at least one there to provide a signal, gives 5 percent for an expected number of 0.1, 1 percent for an expected number of 0.02, and 42 percent for an expected number of 1.0.) Then, given a particle density in the flow of, say, 200 particles/cm<sup>3</sup>, an upper limit may be set for the size of the volume, as follows:

$$\begin{aligned} V_{ob} &\leq 0.1/n = 0.1/200 \text{ cm}^3 \\ &\leq 0.5 \text{ mm}^3 \end{aligned} \quad (3)$$

### 3.2.1 On-Axis

Reducing the observation volume to this size for the on-axis system required design of the specialized lens mask referred to above. As noted, to cover a given range of particle diameters, a smaller fringe spacing is used with the 60-deg mask than would be used with a system having a curve similar to the dashed curve shown in Fig. 2. This is an advantage in that it permits one to use a smaller focused beam radius while retaining several fringes within the region of beam overlap. The observation volume is correspondingly reduced, being proportional to the beam radius squared.

A second advantage of the 60-deg mask is a reduction in dynamic range of signal magnitudes, which not only can relax requirements on the electronics but also makes it easier for the photodetector pinhole to discriminate against extraneous large particle signals, thus shortening the observation volume. Plots of the pedestal  $i_{po}(D)$  and a-c magnitude,  $V_o i_{po}(D)$ , for centered particles versus  $D/\delta$  are shown in Fig. 4 for this mask. These curves were calculated during the course of evaluating Eq. (13) of Ref. 9 for the visibility. For comparison, a dashed line shows the  $D^2$  dependence of the pedestal that would be obtained if all of the diffracted light were collected. The two forward lobes (Airy disks) of the diffraction pattern (one from each illuminating beam), which contain most of the diffracted light power and cover a decreasing angular region in the forward direction with increasing particle diameter, are blocked by the mask for larger particles, giving the attenuated curves of Fig. 4.

Note that the curves of Fig. 4 may be experimentally determined by placing particles in the center of the beam crossover region and measuring the response caused by the moving fringes. The a-c and pedestal components are separated in the electronics by filtering and may be measured separately. For a specific system (including specific laser power, photodetector gain, and electronic processor gain) the vertical axis may be given specific values. An electronic threshold, or "gate" current is selected as shown by the example in Fig. 4. The ratio of signal-to-threshold current is then used to determine the "sample volume" cross-sectional area as a function of particle size, as will be discussed later.

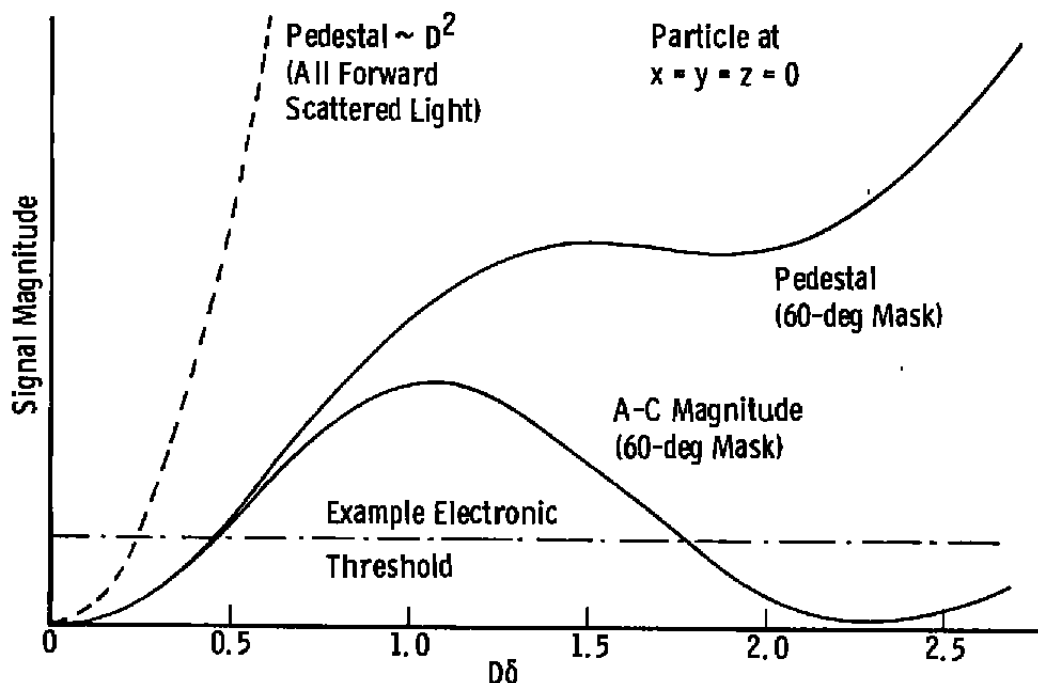


Figure 4. Pedestal and a-c magnitude versus  $D/\delta$  for on-axis light collection.

The length,  $z_{ob}$ , of the observation volume is determined by the aperturing effect of the 60-deg mask in combination with the photodetector pinhole, an effect complicated by the varying angular distribution of the scattered light for different particle sizes. A limitation on how small the pinhole may be made in order to reduce  $z_{ob}$  is that it is desirable that the pinhole not block any light scattered from the particle being sized, since significant blocking of the diffraction pattern beyond the lens mask alters the visibility from that shown by the curve of Fig. 2. A pinhole diameter of 200  $\mu\text{m}$  was selected, which with this system gives a length,  $z_{ob}$ , experimentally determined to be about 20 mm. Since  $b_o = 0.075$  mm, the observation volume of the system is about

$$\begin{aligned}
 V_{ob} &= \pi b_o^2 z_{ob} \\
 &= \pi (0.075)^2 (20) = 0.35 \text{ mm}^3
 \end{aligned}
 \tag{4}$$

which is within the requirement set by Eq. (3).

### 3.2.2 Off-Axis

The arrangement of collection lens, horizontal slit, and photodiode aligned to collect light from an off-axis angle greatly reduces the length,  $z_{ob}$ , of the observation volume. This is an important advantage of an off-axis arrangement. Figure 5 shows an experimental plot of collected light scattered from a glass bead versus the  $z$  coordinate of the bead for the off-axis arrangement. The 120- $\mu\text{m}$  slit was in place for the experiment. A spherical glass bead of 45- $\mu\text{m}$  diameter was placed on a glass slide and moved by a micrometer positioner in the  $z$  direction. The coordinate  $z = 0$  represents the center of the beam crossover region, although

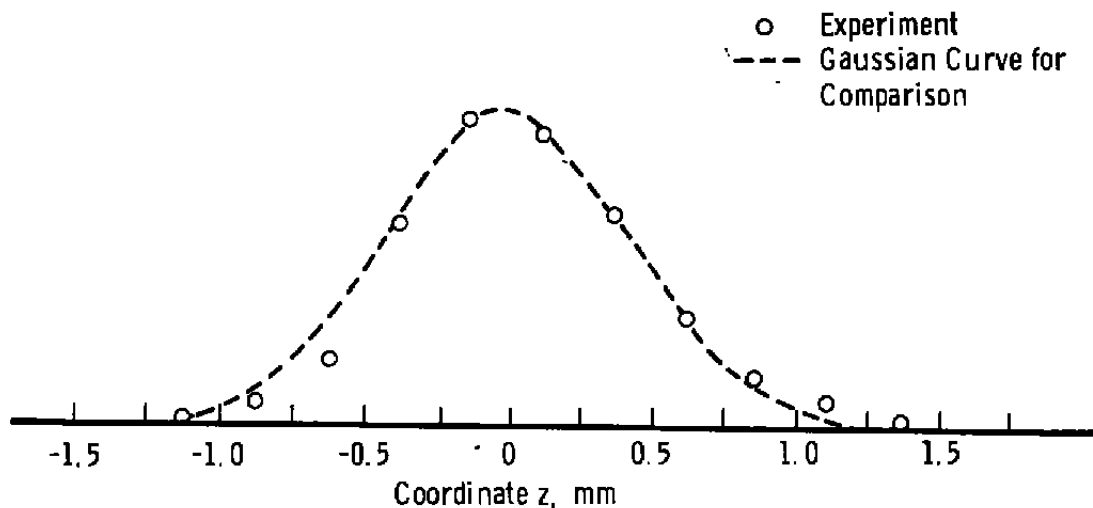


Figure 5. Collected light versus particle  $z$  coordinate, off-axis light collection.

the bead was illuminated by only one beam for this measurement. The collected light curve is approximately Gaussian; for comparison, a Gaussian curve with standard deviation of 0.412 mm is shown as a dotted line. Very similar plots were obtained for beads of 40- and 30- $\mu\text{m}$  diameter. From the plot shown,  $z_{ob}$  for this particular off-axis case is approximately 2.5 mm, giving an observation volume

$$\begin{aligned}
 V_{oh} &= \pi b_o^2 z_{ob} \\
 &= \pi (0.1)^2 (2.5) = 0.079 \text{ mm}^3
 \end{aligned}
 \tag{5}$$

which is more than four times smaller than that for the on-axis case. It could have been made yet smaller had the beam diameter been reduced to that of the on-axis system.

A disadvantage of the off-axis arrangement is that the mechanism by which the light is cut off for particles passing at  $z$  coordinates other than  $z = 0$  is a partial or total blocking of the scattered light by the slit in front of the photodetector. Partial blocking of the light alters the visibility from that shown by the curve in Fig. 3. The result seen when droplets are allowed to freely flow through the crossover region, passing at random  $z$  coordinates, is a broadened instrument response (i.e., a recording of a spread of particle sizes centered on the correct value when a monosize stream of droplets is introduced).

A curve showing the pedestal  $i_{po}$  for centered droplets versus the droplet diameter is shown in Fig. 6 for the off-axis arrangement. This curve was calculated using Mie theory, a

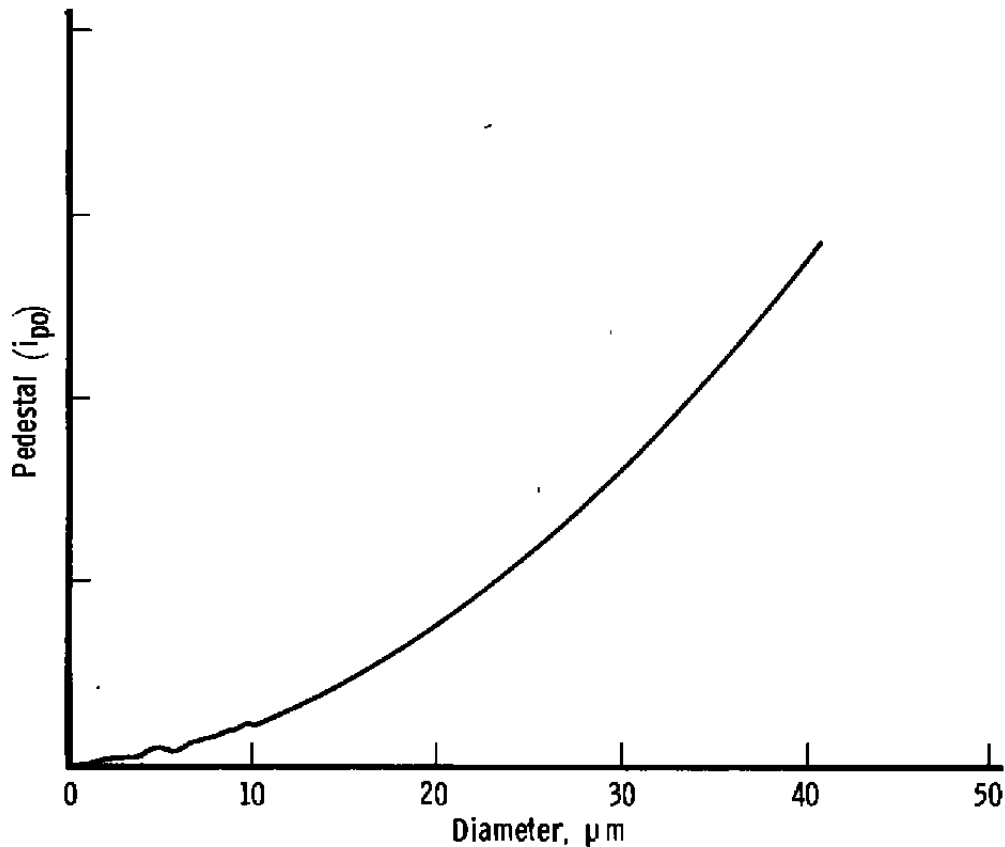


Figure 6. Pedestal versus diameter for off-axis light collection.



droplet refractive index of 1.33,  $\lambda = 0.5145 \mu\text{m}$ , and the illumination polarized in the x direction.

## 4.0 ELECTRONICS

Different electronic signal processing and data acquisition schemes were used with the two optical systems. An analog signal processor was used with the moving fringes of the on-axis optics, and a fully digital approach was used with the stationary fringes of the off-axis system.

### 4.1 ANALOG SYSTEM

An analog electronic signal processor for measuring the visibility of the scattered light waveforms was built on the basis of a modification of the block diagram of Fig. 13 of Ref. 9. The modification was required because particle velocities would have created frequencies beyond the bandwidths of existing analog dividers. In the final design, the photodetector signal was amplified and sent simultaneously to a bandpass filter and to a low-pass filter for separation of the high frequency a-c component from the low frequency pedestal. The a-c component was envelope-detected to produce a signal proportional to the a-c magnitude. The a-c and pedestal components were then both peak-detected to store the maximum values reached individually by the a-c and pedestal components during waveform passage. The ratio of these two values was measured by an analog divider and then converted to digital form by an analog-to-digital converter. This ratio is a valid measure of the peak visibility,  $V_0$ , only for particles passing near the center of the beam crossover region. The consequence is that a high electronic threshold must be used to ensure that only particles passing near center are sized, which in turn means that smaller particles do not get sized because they do not scatter sufficient light for their signals to be above the high threshold. The result is a reduced range of particle sizes that can be covered with a single fringe spacing. This limitation is avoided in the off-axis system, where the optics are designed to collect light only from a narrow region near the center of beam crossover.

A microcomputer based on the 8080 microprocessor was developed to take the individual visibility readings output by the analog-to-digital (A/D) converter and put them in histogram form. Five binary bits were used at the A/D converter output, giving thirty-two different possible visibility readings, numbered 0 to 31 and corresponding to equal increments of visibility from 0 to 1.0. Each of the 32 resolvable visibility readings was used as the address of a memory location in the microcomputer. The content of each memory location was set to zero at the beginning of the data run. Then as each visibility reading, or address, was accepted by the microprocessor, the content of the corresponding memory location was incremented by one count. At the end of the data run, each of the memory addresses then contained the raw count for one bin of the histogram.

A separate, tabletop computer with graphics display was used to control data acquisition, including control of a counter with internal clock to measure the total time required for a data run. The content of each of the 32 memory addresses in the microcomputer, as well as the counter reading, was accepted by the computer at the end of the data run via IEEE-488 standard interface bus cable connections. The computer then made corrections to the raw-count histogram as will be described in Section 5.0 and displayed the corrected size distribution histogram on the graphics screen. Raw data could also be stored on magnetic tape for later analysis.

## 4.2 DIGITAL SYSTEM

The signal output by the photodiode in the off-axis system was amplified using the plug-in vertical amplifier of an oscilloscope. The waveform was then stored and digitized by a commercially available high-speed transient digitizer for subsequent software analysis using a PDP-11 computer.

The computer program which was used calculates the visibility at the peak of the waveform from the equation

$$V = \frac{\text{a-c magnitude}}{\text{pedestal}} = \frac{(I_{mx} - I_{mn})/2}{(I_{mx} + I_{mn})/2} \quad (6)$$

where  $I_{mx}$  is the maximum signal current occurring at the peak of a bright fringe and  $I_{mn}$  is the average value of the two adjoining dark fringes. The waveform is rejected for measurement if its maximum value exceeds the limits of the digitizer's storage array, or if the value of the pedestal  $(I_{mx} + I_{mn})/2$  is not greater than a preselected threshold value. The threshold value is chosen to provide adequate resolution of measurement for small signals. The visibility readings are sorted into bin counts by the program for display in histogram form on a graphics terminal in a manner similar to that of the on-axis electronics display. The histograms could also be stored on magnetic disk for later analysis. A commercial electronic counter was used to measure the run time.

## 5.0 DATA CORRECTIONS

### 5.1 GENERAL

Particle size distribution data are often presented in histogram form. A hypothetical distribution is shown by the curve of Fig. 7 with some of the histogram bars which might be used to represent the distribution. The distribution curve  $f(D)$  is a plot of  $dn/dD$ , where  $n$  is

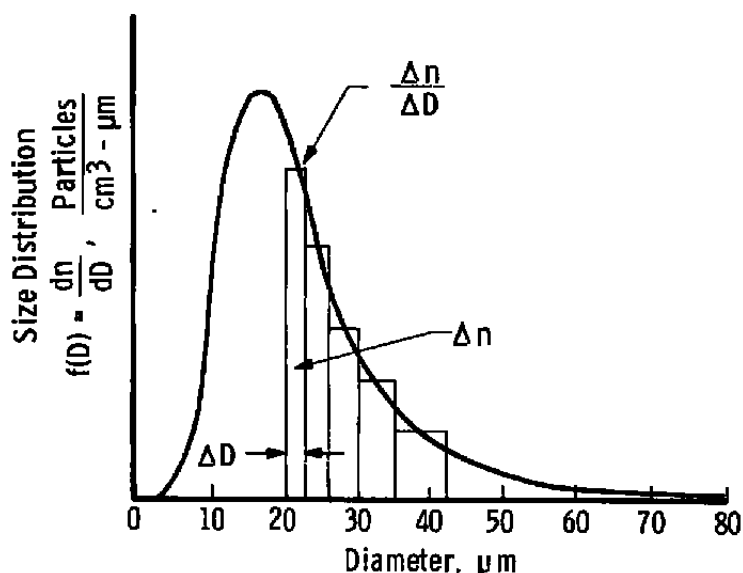


Figure 7. Example log-normal particle size distribution.

the total number density of particles in the flow in particles/cm<sup>3</sup> and  $D$  is the particle diameter in micrometers. Units of  $f(D)$  are therefore particles/cm<sup>3</sup>/μm. The area under the curve is equal to the total number density as follows:

$$\int_0^{\infty} f(D) dD = n \text{ particles/cm}^3 \quad (7)$$

Sometimes the size distribution curve is normalized so that

$$\int_0^{\infty} f(D) dD = 1 \quad (8)$$

In discrete, or histogram form,  $dn/dD$  becomes  $\Delta n/\Delta D$  and

$$\sum \left( \frac{\Delta n}{\Delta D} \right) \Delta D = \sum \Delta n = n \text{ particles/cm}^3 \quad (9)$$

The output of either data acquisition system described in this report is a particle size distribution presented in histogram form on a graphics terminal. Certain corrections must be made to the uncorrected, or raw histogram bar heights before the histogram is displayed, in order that it be in the proper form,  $\Delta n/\Delta D$ . Each uncorrected bar height represents simply the number of particles counted having visibilities falling within the visibility range represented by the bar, or "bin" width. Each raw count must be divided by the volume of

flow sampled to obtain  $\Delta n$  particles/cm<sup>3</sup> and then divided by the bin width,  $\Delta D$ , to obtain  $\Delta n/\Delta D$ .

In the electronics used, each histogram bin has equal width on the visibility axis. Reference to Fig. 2 shows that the visibility curve for the on-axis case is not linear and therefore that bin widths will not be equal on the size axis.

## 5.2 SAMPLE VOLUME

The volume of the flow from which the size distribution is taken is called the sample volume. It is a cylinder of length  $vt_r$  and base area  $A$ , where  $v$  is the flow velocity,  $t_r$  is the time during which the electronic processor is sampling the flow, and  $A$  is the cross-sectional area normal to the flow over which the processor actively responds to measure signals.

The active sample time,  $t_r$ , is given by the equation

$$t_r = T - N_t \tau \quad (10)$$

where  $T$  is the total elapsed time from the beginning of the run until the last particle measurement in the sample is made,  $N_t$  is the total number of measurements made, and  $\tau$  is the processor downtime between measurements (i.e., the time after each measurement during which the processor is off-line to record the data point). If a particle passes through the crossover region during the downtime, the processor does not respond to it, and therefore, the time  $N_t\tau$  must be subtracted from  $T$  in the determination of the volume of air sampled.

The active cross-sectional area,  $A$ , varies with particle size. Although small particles must pass close to the center of the beam crossover region for the scattered light signal to exceed the processor's threshold and trigger a measurement, larger particles may pass further out and still trigger a measurement, thus defining a larger active area.

### 5.2.1 On-Axis

The aperturing effect of the photodetector pinhole was designed in this system to occur outside the region of beam crossover so that visibilities of particles being sized would not be altered by the pinhole. The size of the cross-sectional area in this case is determined primarily by the fall-off in illuminating intensity contained in the exponential factor in Eq. (1) and can be calculated as follows.

The a-c magnitude signal, separated out in the electronics, is used as the reference signal to be compared with the selected threshold to trigger a measurement. The a-c (cosine) magnitude is here designated  $i_a$  and from Eq. (1) is given by

$$i_a = V_o i_{po}(D) \exp \left[ -2/b_o^2 (x^2 + y^2 + z^2 \alpha^2/4) \right] \quad (11)$$

where  $V_o i_{po}(D)$  is the a-c magnitude for a centered particle of diameter  $D$  and is given by the curve in Fig. 4. For particles moving in the  $y$ -direction (defined in Fig. 1),  $i_a$  reaches a maximum value where the particle crosses the  $xz$  plane ( $y = 0$ ), and the active cross-sectional area is determined in this plane.

Following a derivation in Ref. (12), in the  $y = 0$  plane Eq. (11) may be written

$$i_a = V_o i_{po}(D) \exp \left\{ -2 \left[ \left( x^2/b_o^2 \right) + \left( z^2/b_3^2 \right) \right] \right\} \quad (12)$$

where  $b_3 = 2b_o/\alpha$ . This equation yields elliptical contours of constant signal amplitude,  $i_a$ , in the  $y = 0$  plane, described by

$$\left( x/b_o \right)^2 + \left( z/b_3 \right)^2 = \ln \left[ \left( V_o i_{po}(D)/i_a \right)^{1/2} \right] \quad (13)$$

and the area within the contour specified by setting  $i_a$  equal to the threshold current,  $i_G$ , gives the cross-sectional area,  $A$ , for a particle of diameter  $D$ :

$$A = \pi b_o b_3 \ln \left[ \left( V_o i_{po}(D)/i_G \right)^{1/2} \right] \quad (14)$$

### 5.2.2 Off-Axis

In the off-axis system, the aperturing effect of the photodetector slit is the primary mechanism which determines the  $z$ -direction dimension of the active cross-sectional area,  $A$ . The fall-off in collected light with the coordinate  $z$  for particles passing up or downstream of the  $z = 0$  point is shown in Fig. 5. This response curve is approximately Gaussian, with standard deviation  $\sigma = 0.412$  mm. The curve has fallen to  $1/e^2$  times its maximum value at  $z = 2\sigma = 0.824$  mm, much faster than the fall-off in illuminating intensity with  $z$  given by Eq. (1). The containment of the active cross-sectional area to a region near the center of the beam crossover region means that the maximum pedestal  $i_p$  for particles moving in the  $y$  direction occurs, as does the maximum a-c component,  $i_a$ , at  $y = 0$ . The Gaussian shape of

the response curve of Fig. 5 further leads to the approximation that the pedestal  $i_p$  in the  $y = 0$  plane may be given by

$$i_p = i_{po}(D) \exp \left\{ -2 \left[ \left( x^2 / b_o^2 \right) - \left( z^2 / b_3^2 \right) \right] \right\} \quad (15)$$

which is similar to Eq. (12) for the a-c magnitude,  $i_a$ , in the on-axis system, but where  $b_3$  is here equal to the experimental value 0.824 mm.

As in Eq. (14) above, the cross-sectional area,  $A$ , is given by

$$A = \pi b_o b_3 \ell_n \left[ \left( i_{po}(D) / i_G \right)^{1/2} \right] \quad (16)$$

where the pedestal current is used as the reference signal to be compared with the threshold current,  $i_G$ .

A plot of the cross-section,  $A$ , versus diameter,  $D$ , calculated using Eq. (16) is shown as the solid line in Fig. 8. The curve has been smoothed below  $10 \mu\text{m}$  to eliminate oscillations that would otherwise occur due to the oscillations in the  $i_{po}$  versus  $D$  curve as shown in Fig. 6. The system's resolution below  $10 \mu\text{m}$  is not sufficient to make accounting for such oscillations necessary.

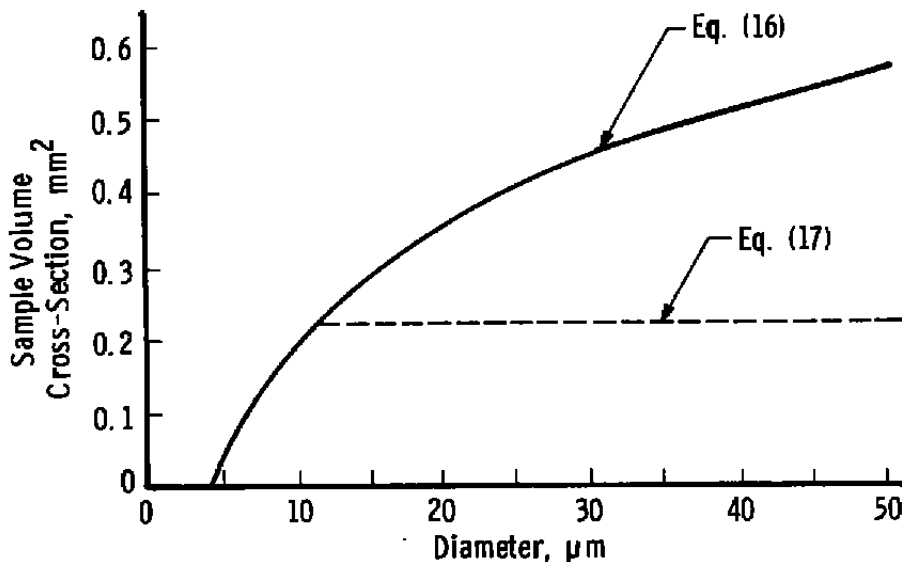


Figure 8. Sample volume cross-sectional area versus particle diameter for off-axis system.

If, in addition to the lower limit on the pedestal  $i_G$ , an upper limit is also placed, say  $i_{pmx}$ , such that signals whose pedestals exceed  $i_{pmx}$  are rejected, then the cross-section,  $A$ , becomes the annular area between two ellipses; the area within an inner ellipse must be subtracted since particles passing there are unacceptable because of too great a signal magnitude. The area,  $A$ , becomes

$$\begin{aligned} A &= \pi b_o b_3 \ell_n \left\{ \left[ i_{po}(D) / i_G \right]^{1/2} \right\} - \pi b_o b_3 \ell_n \left\{ \left[ i_{po}(D) / i_{pmx} \right]^{1/2} \right\} \\ &= \pi b_o b_3 \ell_n \left[ \left( i_{pmx} / i_G \right)^{1/2} \right] \end{aligned} \quad (17)$$

The area  $A$  becomes a constant given by Eq. (17) for droplet diameters such that

$$i_{po}(D) \geq i_{pmx}$$

This case is shown as the dotted line in Fig. 8. Although this result of a constant sample volume independent of particle size is based on a mathematical model, it should hold for a useful range of particle diameters. It should also be noted that the sensitive cross section,  $A$ , is annular, which means that large particles passing through the center of the crossover region are rejected for measurement, although this region is normally where the best measurements relating visibility to size are made.

### 5.3 CORRECTIONS SUMMARY

In summary, the correction to each histogram raw bin count is made as follows:

$$\left( \frac{\Delta n}{\Delta D} \right)_i = \frac{N_i}{A_i v_i t_r (\Delta D)_i} \cdot \text{particles/cm}^3/\mu\text{m} \quad (18)$$

where

$\left( \frac{\Delta n}{\Delta D} \right)_i$  is the corrected bin count (i.e., the  $i$ th bar height),

$N_i$  is the raw bin count for the  $i$ th bin,

$A_i$  is the sample volume cross-sectional area in square centimeters for the particle size corresponding to the  $i$ th bin,

$v_i$  is the velocity in centimeters per second of those particles whose size corresponds to the  $i$ th bin,

$t_r$  is the time during which the signal processor is online, sampling the flow, and

$(\Delta D)_i$  is the width of the  $i$ th bin in micrometers.

If only the shape of the distribution is desired (i.e., only the relative frequency of occurrence of each size), rather than an absolute count in particles/cm<sup>3</sup>, and if it is assumed that all particles have the same velocity, then the factor  $v_i t_r$  in Eq. (18) may be omitted. Further, if bin widths are all the same on the size axis and the cross-sectional area,  $A$ , is also a constant, then no corrections are required to obtain a relative distribution curve. In fact, for the off-axis system being described in this report, these factors are approximately constant, and the raw data may be presented alone to give relative distribution curves.

## 6.0 MONOSIZE RESPONSE: THEORETICAL CONSIDERATIONS

An important characteristic of a particle-sizing system is its response to a monosize (monodisperse) flow of particles. The narrowness of this response determines system resolution (i.e., the ability of the system to distinguish a bimodal distribution when the two modes, or peaks, are closely spaced). Correspondingly, it determines the capability of the system to reproduce a steeply rising or falling distribution curve.

The Berglund-Liu vibrating orifice droplet generator is capable of producing a highly monosize flow of droplets down to diameters on the order of 1  $\mu$ m; this capability enables one to conveniently observe the monosize response while calibrating the system. When the monosize response is measured, it is important that the test particles be permitted to flow freely throughout the active measurement region of the instrument, rather than being constrained to flow only through some one favorable point.

When an actual distribution,  $f(D)$ , is measured, the distribution recorded by the instrument (i.e., the system output), say  $g(D)$ , is given by the convolution of the actual distribution,  $f(D)$ , and the monosize response of the system,  $h(D)$ :

$$g(D) = \int_{-\infty}^{\infty} h(D - D_o) f(D_o) dD_o \quad (19)$$

In this formulation,  $h(D)$  is the response to a "unit" monosize flow; i.e., there is one particle/cm<sup>3</sup> in the flow:  $\int_{-\infty}^{\infty} h(D) dD = 1$ . It is also assumed that the monosize response is independent of the diameter of the monosize droplets, although this is probably not actually the case.



An example illustrating Eq. (19) is shown in Figs. 9a and b. A hypothetical instrument monosize response is shown in Fig. 9a, here taken simply to be a Gaussian response. A hypothetical log-normal size distribution,  $f(D)$ , is graphed as the solid curve in Fig. 9b. The result of numerically convolving  $f(D)$  and  $h(D)$  is the dashed curve,  $g(D)$ , shown in Fig. 9b. It is seen that the instrument in this case can reproduce quite well the right-hand slope of  $f(D)$  but cannot reproduce the steeper, left-hand slope. The monosize response curves for the instruments described in this report are discussed in Section 7.1.

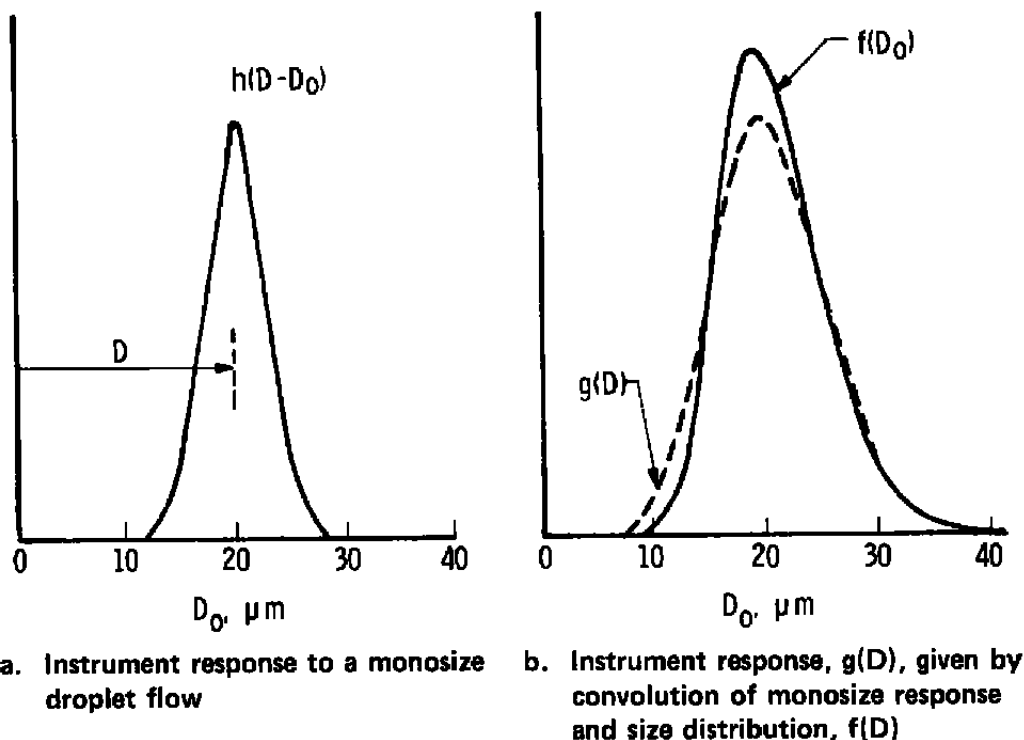


Figure 9. Instrument response.

## 7.0 DATA RESULTS

### 7.1 LABORATORY DATA

Visibility measurements with the on-axis system were obtained from glass spheres (microbeads) placed on a glass slide, and from water droplets and oleic acid droplets produced by a Berglund-Liu monosize droplet generator. Experimental data shown in Fig. 2 are examples of glass bead data.

The data acquisition electronics used with the on-axis system measured the visibilities, converted to particle size through the solid curve of Fig. 2, and then displayed a size

distribution histogram. Figure 10 shows the result of measuring 100 droplets each of five different sizes produced by the droplet generator. The drops flowed freely throughout the beam crossover region during the test and were not constrained to a single, favorable path. In effect, Fig. 10 shows the monosize response (see Section 6.0) of the instrument at five different particle diameters. The monosize response is quite narrow for this on-axis system, giving good resolution, adequate to easily resolve sizes  $5\text{ }\mu\text{m}$  apart in this range.

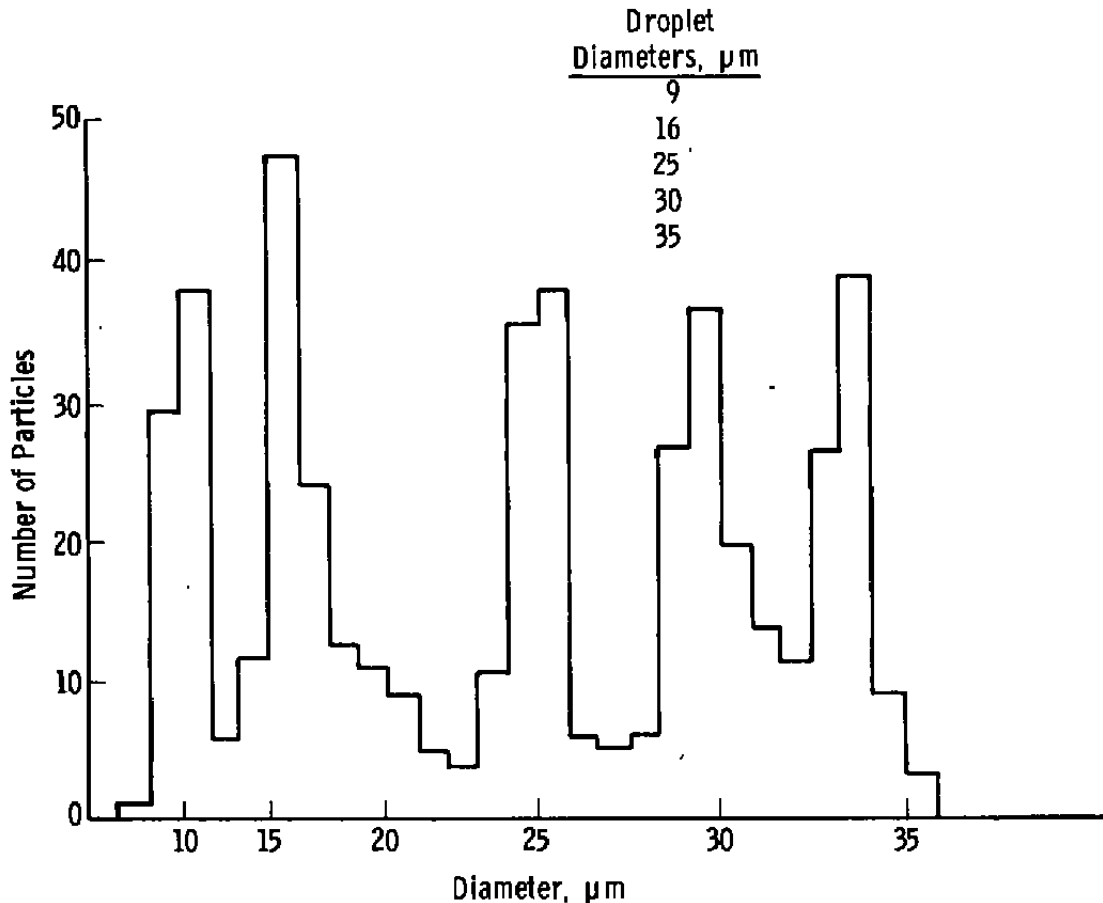


Figure 10. On-axis system response to five different monosize droplet flows.

The experimental data of Fig. 3 are examples of laboratory data taken using the off-axis system and water and oleic acid droplets produced by the Berglund-Liu generator.

The monosize response of the off-axis system was broader than that of the on-axis system. An example is shown in Fig. 11, for a monosize stream of droplet diameter =  $9.2\text{ }\mu\text{m}$ . The broader response was anticipated since the off-axis system achieves its smaller observation volume by the photodetector slit aperture's partially or completely blocking

scattered light originating anywhere except from a small region at the center of the beam crossover region. The resultant partial blocking of the scattered light from many signals alters the visibility for these signals from the calibration curve of Fig. 3 and gives a broadened monosize response.

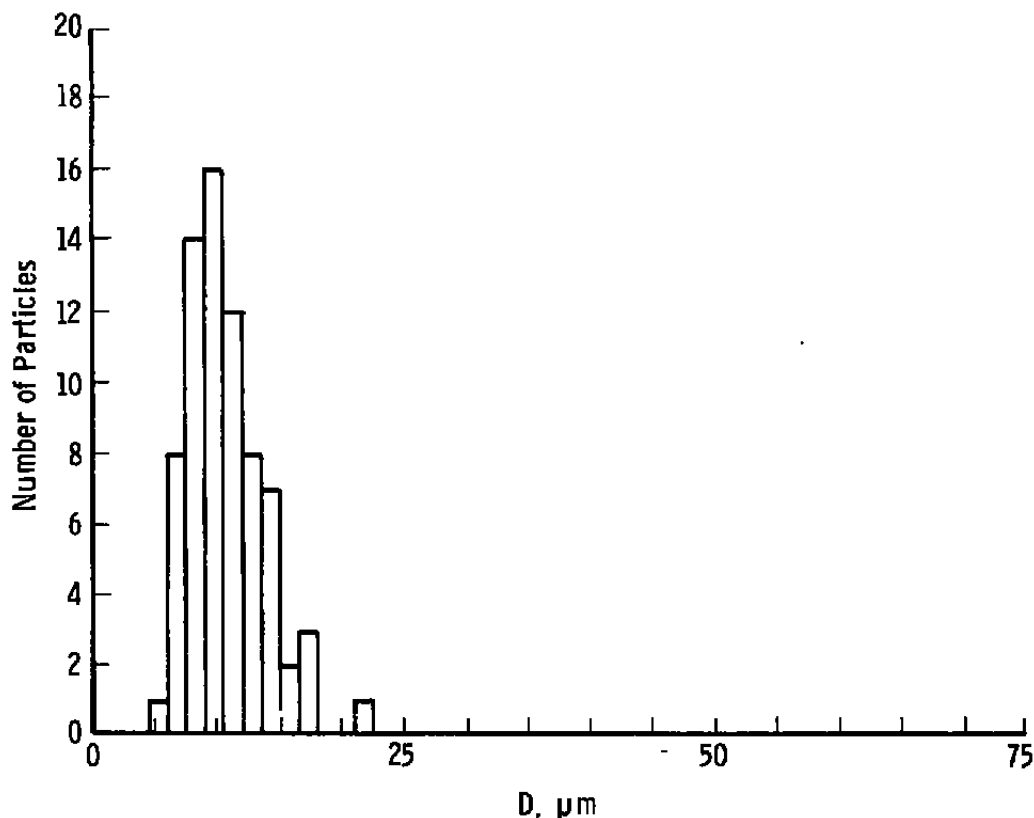


Figure 11. Off-axis system response to monosize droplet flow, diameter =  $9.2 \mu\text{m}$ .

## 7.2 WIND TUNNEL DATA

The on-axis system was installed first for testing in the ETF R1D icing studies wind tunnel to obtain water droplet measurements. The tunnel has a 3-ft outside diameter with the droplets carried within a 12-in.-diam flow. Droplet diameters were measured in the range from 5 to  $80 \mu\text{m}$ . Particle number densities ranged up to a few hundred particles/ $\text{cm}^3$ . Velocities in the flow exceeded 100 m/sec. Measurements produced inconsistent results, which are attributed to a high probability that there was more than one particle at a time in the observation volume.

The off-axis system was designed to provide the necessary smaller observation volume and was installed in the tunnel after laboratory calibration. An example of a data histogram obtained for a particular set of tunnel and spray nozzle conditions is shown in Fig. 12. The histogram shown displays raw data. Data corrections discussed in Section 5.0 of this report were not necessary to show the relative shape of the distribution, since bin widths are uniform along the size axis (due to the linear calibration curve shown in Fig. 3) and since the sample volume cross-sectional area is approximately constant for sizes greater than  $10\text{ }\mu\text{m}$  (shown as the dashed line in Fig. 8). To attempt to correct for cross-sectional area variations below  $10\text{ }\mu\text{m}$  would only have served to disproportionately amplify noise counts in this case.

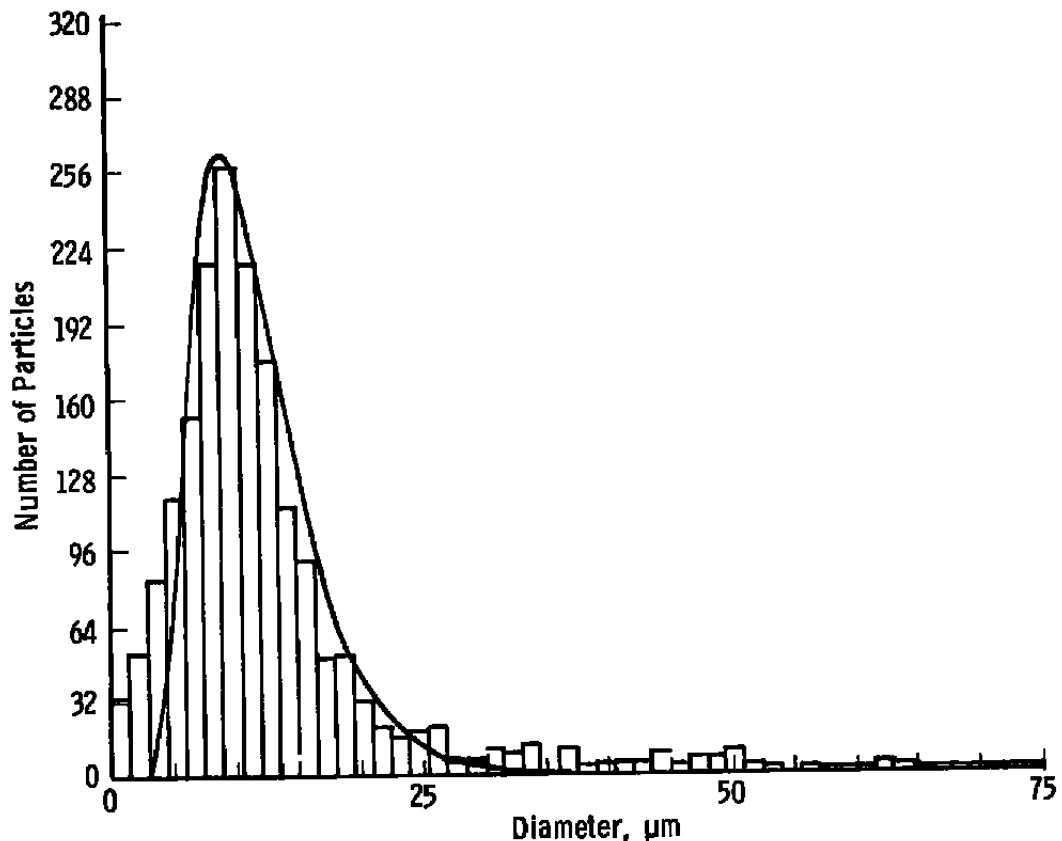


Figure 12. Log-normal curve fit to measured tunnel size distribution.

The sizes of spray droplets from a nozzle are often modeled by a log-normal distribution, given by

$$\frac{\Delta n}{\Delta D} = \frac{1}{D \ell_n a_2 \sqrt{2\pi}} \exp \left[ -\frac{1}{2} \left( \frac{\ell_n D - \ell_n a_1}{\ell_n a_2} \right)^2 \right] \quad (20)$$

where  $n$  is the particle number density,  $D$  is the particle diameter,  $\alpha_1$  is the geometric mean, and  $\alpha_2$  is the geometric standard deviation. The solid curve in Fig. 12 is a log-normal curve with parameters chosen to fit the experimental data. Parameters used were  $\ln \alpha_1 = 2.4$  and  $\ln \alpha_2 = 0.4$ . A multiplying factor was then used to give the log-normal curve the same height as the histogram.

The fit fails above about  $30 \mu\text{m}$ , possibly because of droplets combining to form bigger drops after an initial log-normal distribution was produced by the nozzle. The fit also fails for droplets smaller than about  $6 \mu\text{m}$ , which would be expected for a system having a monosize response as shown in Fig. 11, where system resolution is not sufficient to follow the steep rise of the log-normal model. (See the example calculation illustrated in Fig. 9.)

An alternative model sometimes used for water sprays is the Nukiyama-Tanasawa distribution, given by

$$\frac{\Delta n}{\Delta D} = a D^2 \exp \left[ -b D^q \right] \quad (21)$$

where  $a$ ,  $b$ , and  $q$  are parameters chosen to fit the experimental data. The solid curve in Fig. 13 shows a Nukiyama-Tanasawa curve fit to the same data histogram as that shown in Fig. 12. Parameters used were  $b = 6.67 \times 10^{-4}$  and  $q = 3$ , with the factor " $a$ " value chosen to give the curve the same height as the histogram. The histogram seems better fit by the log-normal model than by the Nukiyama-Tanasawa in this case.

The data agree reasonably well with size distributions determined from holograms taken of the droplet flow under similar tunnel and nozzle conditions. For comparison with the holographic data, the PSI histogram bin widths were changed from  $1.5$  to  $4.5 \mu\text{m}$ ; i.e., raw counts from every three bins were combined (summed) into one equivalent bin having a width equal to the combination of three original bins. This provides better comparison with the holographic data histograms, which have bins  $5 \mu\text{m}$  wide.

Figures 14 and 15 each show PSI data as a solid line and holographic data as a broken line. Each holographic histogram has been multiplied by a factor to approximately equalize its height with the corresponding PSI histogram, since it is the relative distribution that is being compared. In Fig. 14 the PSI data were taken for a water flow of  $0.1 \text{ gal/min}$  and a nozzle air pressure of  $29 \text{ psi}$ . For the holographic data, the conditions were similar, being  $0.111 \text{ gal/min}$  and  $50.31 \text{ psi}$ .

In Fig. 15 the conditions for the PSI data were  $0.044 \text{ gal/min}$  and  $144.09 \text{ psi}$  and for the holographic data were  $0.047 \text{ gal/min}$  and  $112.5 \text{ psi}$ .

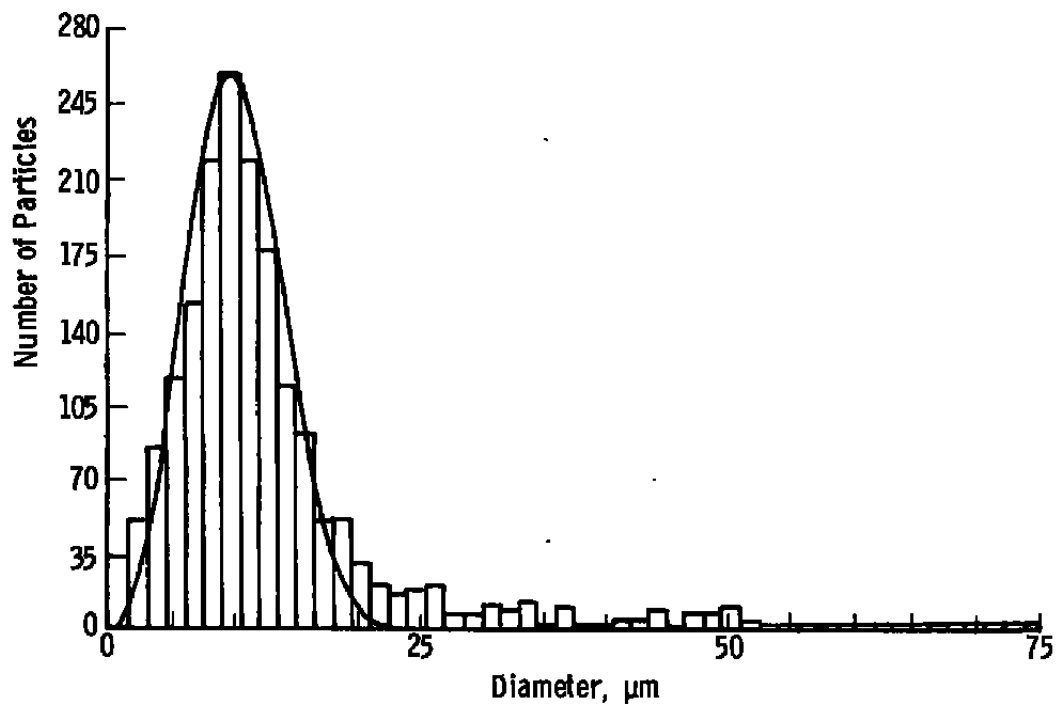


Figure 13. Nukiyama-Tanasawa curve fit to measured tunnel size distribution.

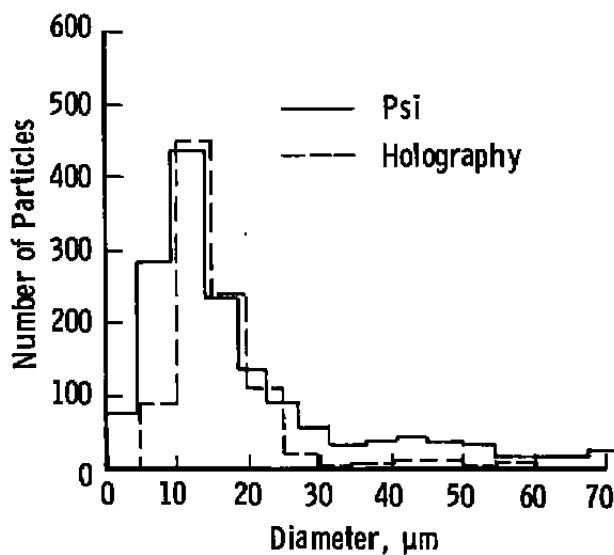


Figure 14. Comparison of particle size interferometer with holography data.

The comparison of PSI and holographic data is reasonably good. It is assumed that the reason the PSI shows a higher count of particles less than 10  $\mu\text{m}$  in diameter is that holography is less sensitive to the smaller particles in that range.

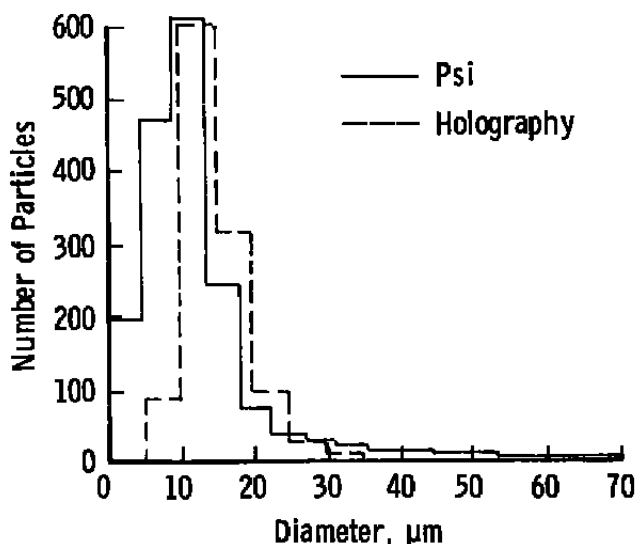


Figure 15. Comparison of particle size interferometer with holography data.

## 8.0 CONCLUSIONS

A particle-sizing interferometer was designed and built for use in the AEDC subscale icing studies facility, RID. Two designs were evaluated, one with forward-scatter, on-axis light collection, and one with collection of the light from 12 deg off-axis in the forward direction. Laboratory evaluation showed the on-axis system to have the better capability to resolve between closely spaced sizes. The requirement of a small observation volume to discriminate against multiple-particle signals, however, dictated the use of the off-axis system to obtain correct results in the wind tunnel. Data obtained in the tunnel compared favorably with holographic data obtained under similar spray nozzle conditions of air pressure and water flow.

Water droplets were sized in the range from 5 to 80  $\mu\text{m}$  while droplet velocities measured in the air flow were in excess of 100 m/sec. Number densities in the flow were a few hundred droplets per cubic centimeter.

Particle size interferometry offers an attractive means of *in situ* sizing of droplets in the range of diameters from a few micrometers to a few hundred micrometers. The method

features rapid, online data reduction and simultaneous velocity measurement. However, it shares with other single-particle, *in situ* instruments the requirement for low to moderate particle number densities.

Further investigation will be required to define the applicability of particle sizing interferometry to irregularly shaped particles.

## REFERENCES

1. Farmer, W. M. "Measurement of Particle Size, Number Density, and Velocity Using a Laser Interferometer." *Applied Optics*, Vol. 11, No. 11, November 1972, pp. 2603-2612.
2. Robinson, D. M. and Chu, W. P. "Diffraction Analysis of Doppler Signal Characteristics for a Cross-Beam Laser Doppler Velocimeter." *Applied Optics*, Vol. 14, No. 9, September 1975, pp. 2177-2183.
3. Roberds, D. W. "Electronic Instrumentation for Interferometric Particle Sizing." Ph.D. Dissertation, The University of Tennessee, Knoxville, 1975.
4. Durst, F. and Eliasson, B. "Properties of Laser Doppler Signals and Their Exploitation for Particle Size Measurements." Paper presented at LDA-Symposium 1975, Copenhagen, Denmark, August 1975.
5. Hong, N. S. and Jones, A. R. "A Light Scattering Technique for Particle Sizing Based on Laser Fringe Anemometry." *Journal of Physics D: Applied Physics*, Vol. 9, 1976, pp. 1839-1848.
6. Adrian, R. J. and Orloff, K. L. "Laser Anemometer Signals: Visibility Characteristics and Application to Particle Sizing." *Applied Optics*, Vol. 16, No. 3, March 1977, pp. 677-684.
7. Chu, W. P. and Robinson, D. M. "Scattering from a Moving Spherical Particle by Two Crossed Coherent Plane Waves." *Applied Optics*, Vol. 16, No. 3, March 1977, pp. 619-626.
8. Roberds, D. W. "Particle Sizing Using Laser Interferometry." *Applied Optics*, Vol. 16, No. 7, July 1977, pp. 1861-1868.
9. Roberds, D. W., Bomar, B. W., and Menzel, R. W. "Interferometric Particle Sizing." AEDC-TR-77-116 (AD-A053729), April 1978.



10. Bachalo, W. D. "Method for Measuring the Size and Velocity of Spheres by Dual-Beam Light-Scatter Interferometry." *Applied Optics*, Vol. 19, No. 3, February 1980, pp. 363-370.
11. Berglund, R. N. and Liu, B. Y. H. "Generation of Monodisperse Aerosol Standards." *Environmental Science and Technology*, Vol. 7, No. 2, February 1973, pp. 147-153.
12. Yule, A. J., Chigier, N. A., Atakan, S., and Ungut, A. "Particle Size and Velocity Measurement by Laser Anemometry." *Journal of Energy*, Vol. 1, No. 4, July -August 1977, pp. 220-228.